# Experimental Indicators of Current Unbalance in Building-Integrated Photovoltaic Systems

Gianfranco Chicco, *Senior Member, IEEE*, Fabio Corona, Radu Porumb, *Member, IEEE*, and Filippo Spertino, *Member, IEEE*

***Abstract*—Unbalance of the three-phase currents in photovoltaic (PV) systems may depend on structural aspects of the installation, the effect of partial shading, or both. In this paper, a number of unbalance indicators are calculated starting from data that are measured during experimental analyses on a real building-integrated PV system that represents different types of unbalance. Detailed information is obtained from indices that identify the balance and unbalance components that are also in the presence of waveform distortion. These indices extend the current definitions of unbalance given in the power quality standards. The results show that the unbalance cannot be considered negligible, even with no single-phase inverters and is more significant if nonlinear loads add a contribution to both harmonic distortion and unbalance seen from the distribution transformer.**

***Index Terms*—Current, harmonic distortion, photovoltaic (PV) systems, symmetrical components (SCs), unbalance indicator.**

## I. Introduction

AFTER a period of expansion of the installation of grid-connected photovoltaic (PV) systems, mainly ground mounted, in a number of European countries, the recent evolution of the feed-in tariffs, particularly in Italy [1], has brought a sudden decrease in investment in multimegawatt PV plants. On the other hand, the self-production of electricity by both small ($<$20 kW$_p$) and mid-size (up to 1 MW$_p$) PV systems, such as those for single family, commercial, and industrial users that are installed in building integration (BIPV), is increasing. Currently, the new policies, which are aimed to construct more energy-efficient buildings, can stimulate the development of distributed generation (DG) in the cities. A key issue is the study of the DG impact on the grid, both at low-voltage (LV) and medium-voltage (MV) levels, including power quality (PQ) aspects [2].

In this new scenario, with a multitude of PV systems operating in an urban environment, the BIPV systems are intrinsically affected by partial shading. Roofs in a city are full of obstacles (e.g., antennas, chimneys, trees, poles, nearby buildings, or structures), which are unavoidable for the PV plant installer. Thus, the problem of partial shading over the PV modules can have a high impact on PQ. Moreover, PV plants with a single-phase connection on the LV side of the grid supposedly will be aggregated to each phase of the three-phase distribution network. Therefore, it will be difficult to obtain a perfectly balanced configuration. For example, the number of single-phase inverters per each phase may be different or the exposure of the PV arrays to the sun may vary (towards the south, east, or west).

The focus of this paper is to characterize the unbalance that is produced by a PV system connected to the grid, which highlights three typologies of unbalance: 1) "structural unbalance," 2) "unbalance from partial shading," and 3) "mixed unbalance." More emphasis is given to the effect of the partial shading on the PV arrays because this could be the most frequent scenario in practical installations. A PV system that is installed on an industrial site is analyzed, in which all three of the unbalance typologies are observable. Without shading, the possible "structural unbalance" is caused by how the PV field is distributed over the three phases at the PV generator output. Then, two PV arrays with periodic partial shading are studied. Finally, mixed unbalance is considered, taking into account the currents absorbed by the loads.

Unbalance is analyzed using PQ indicators computed by decomposing the three-phase currents, with or without the use of the symmetrical components (SCs) [3]. These indicators are more detailed than those currently adopted in PQ standards, as they make it possible to determine more accurate values of the unbalance indicators taking into account the harmonic distortion of the waveforms.

Section II of this paper recalls the unbalance indicators that are used in PQ analysis. Section III presents the real PV system studied. Section IV shows and discusses the experimental results. Section V reports some suggestions to extend the unbalance indicators in the PQ standards. Section VI contains the conclusions.

## II. Unbalance Indicators

Various unbalance indicators have been defined for the system voltages and currents. The large majority of the literature studies and standards consider *voltage* unbalance in three-phase systems, which occurs due to unsymmetrical voltage supply among the phases, unsymmetrical line parameters among the phases, or unbalanced loads.

Manuscript received November 4, 2013; revised January 13, 2014; accepted February 16, 2014. Date of publication March 12, 2014; date of current version April 18, 2014. This work was supported by the European Union Seventh Framework Programme FP7/2007-2013 under Grant 309048, Project Smart and Sustainable Insular Electricity Grids Under Large-Scale Renewable Integration (SiNGULAR).

G. Chicco, F. Corona, and F. Spertino are with the Power and Energy Systems Group, Department of Energy, Politecnico di Torino, 10129 Torino, Italy (e-mail: gianfranco.chicco@polito.it; fabio.corona@polito.it; filippo.spertino@polito.it).

R. Porumb is with the Faculty of Power Engineering, Universitatea Politehnica din Bucuresti, 060042 Bucharest, Romania (e-mail: radu.porumb@upb.ro).

Digital Object Identifier 10.1109/JPHOTOV.2014.2307491

One of the effects of unbalance is the current (and losses) increase in one of the phases, which leads the related conductor to reach its temperature limit before the other phases. The classical example on an induction motor links unbalance with a *derating* factor (the ratio between the maximum output powers in unbalance and balance conditions), such that no conductor exceeds its thermal limits. A NEMA recommendation [4] indicates a reduction of the induction motor capacity to 75% for a 5% voltage unbalance at fundamental frequency.

In [5], three transformerless PV inverter topologies for three-phase grid connection are compared also in terms of their effects of unbalance conditions. Structural unbalance between the phases leads to a common-mode voltage component that is influenced by the difference between the inductors on the phases.

In pulse width modulated voltage-source converter applications, input-voltage unbalances cause second harmonic voltage components to be injected onto the dc link. The unbalance compensation solution in [6] is designed to minimize the amount of second harmonic, regardless of the input voltage unbalance types, using the definitions taken from [7].

Unbalanced voltage variations that are caused by PV power drop because of moving clouds are analyzed in [8] in a small geographic area based on simulations. In [9], a PQ index combines voltage unbalance and harmonic distortions, without measuring individual harmonic distortions in each phase of the power supply.

In [10] and [11], instantaneous power flows are analyzed for three-phase unbalanced systems with sinusoidal voltages and currents. The instantaneous power approach in [12] determines the unbalance power from the IEEE Std. 1459 definition and from a different expression determined from a study on an unbalanced linear load.

For PV generation, a key point is to characterize the *current* output, as the behavior of the PV modules is qualitatively close to a current generator (as in the basic PV circuit models with an ideal current generator [13], [14]). This point of view makes PV systems relatively different with respect to other plants in which unbalance has been quantified, providing the rationale to study the unbalance with reference to the system currents.

This section recalls a number of unbalance indicators that are defined in relation to the system phase currents. The unbalance indicators are partitioned into two groups:

1) indicators calculated from variables transformed into SCs;
2) indicators calculated from variables *not* transformed into SCs.

The transformed current components that are used to define the indicators are illustrated in the following sections.

### *A. Current-Based Components From the Symmetrical Component Transformation*

For the three phases $a$, $b$, and $c$, using the phasor notation, the vector of the complex numbers representing the phase current, at the harmonic order $h$, is

$$\bar{I}^{(h)} = \left| \begin{array}{ccc} \bar{I}_a^{(h)} & \bar{I}_b^{(h)} & \bar{I}_c^{(h)} \end{array} \right|. \tag{1}$$

Moreover, $\bar{I}_n^{(h)}$ indicates the neutral current phasor.

By defining the operator $\alpha = e^{j2\pi/3}$, the SC transformation matrix [3] is denoted as

$$\mathbf{T} = \frac{1}{3} \begin{vmatrix} 1 & \alpha & \alpha^2 \\ 1 & \alpha^2 & \alpha \\ 1 & 1 & 1 \end{vmatrix}. \tag{2}$$

The matrix $\mathbf{T}$ is directly used in the SCB method [15] to obtain the transformed currents

$$\left| \begin{array}{ccc} \bar{I}_{T1}^{(h)} & \bar{I}_{T2}^{(h)} & \bar{I}_{T3}^{(h)} \end{array} \right|^{\mathrm{T}} = \mathbf{T} \cdot \left| \begin{array}{ccc} \bar{I}_a^{(h)} & \bar{I}_b^{(h)} & \bar{I}_c^{(h)} \end{array} \right|^{\mathrm{T}} \tag{3}$$

where the subscripts $T_1, T_2$, and $T_3$ represent the positive, negative, and zero components of the transformed variables, respectively. The rationale of the SCB method is that under *balanced* conditions the following conditions are verified for $m = 1, 2, \ldots, \infty$.

1) For $h = 3m - 2$, only the positive-sequence component of each $h$th harmonic phasor is nonzero.
2) For $h = 3m - 1$, only the negative-sequence component of each $h$th harmonic phasor is nonzero.
3) For $h = 3m - 3$, only the zero-sequence component of each $h$th harmonic phasors is nonzero.

In other words, if the three-phase system is balanced, the phasors of the harmonic orders 1, 4, 7, ... present only the positive-sequence component, while for the harmonic orders 2, 5, 8, ... there is only the negative-sequence component, and for triplen harmonics (i.e., 3, 6, 9, ...) only the zero-sequence component exists. The Euclidean sum of these components can be taken as an index of how balanced the system is. Any unbalance would result in the appearance of positive and/or negative-sequence terms for the various harmonics [16].

Hence, the transformed currents can be used to define the balance phase current component $I_p^{(b)}$, unbalance component $I_p^{(u)}$, and distortion component $I_p^{(d)}$ as follows:

$$I_p^{(b)} = \sqrt{\sum_{m=1}^{\infty} \left[ \left( I_{T1}^{(3m-2)} \right)^2 + \left( I_{T2}^{(3m-1)} \right)^2 + \left( I_{T3}^{(3m-3)} \right)^2 \right]} \tag{4}$$

$$I_p^{(u)} = \sqrt{\sum_{m=1}^{\infty} \left[ \begin{array}{l} \left( I_{T2}^{(3m-2)} \right)^2 + \left( I_{T3}^{(3m-2)} \right)^2 + \left( I_{T1}^{(3m-1)} \right)^2 + \\ \left( I_{T3}^{(3m-1)} \right)^2 + \left( I_{T1}^{(3m-3)} \right)^2 + \left( I_{T2}^{(3m-3)} \right)^2 \end{array} \right]} \tag{5}$$

$$I_p^{(d)} = \sqrt{\sum_{h=2}^{\infty} \left[ \left( I_{T1}^{(h)} \right)^2 + \left( I_{T2}^{(h)} \right)^2 + \left( I_{T3}^{(h)} \right)^2 \right]}. \tag{6}$$

Furthermore, the balance phase current at fundamental frequency is expressed as

$$I_p^{(b1)} = I_{T1}^{(1)} \tag{7}$$

and the balance phase current distortion component is

$$I_p^{(bd)} = \sqrt{\left( I_p^{(b)} \right)^2 - \left( I_p^{(b1)} \right)^2}. \tag{8}$$

In the same way, it is possible to separate the fundamental component also for the unbalance component

$$I_p^{(u1)} = \sqrt{\left(I_{T2}^{(1)}\right)^2 + \left(I_{T3}^{(1)}\right)^2} \tag{9}$$

from the unbalance phase current distortion component

$$I_p^{(ud)} = \sqrt{\left(I_p^{(u)}\right)^2 - \left(I_p^{(u1)}\right)^2}. \tag{10}$$

Some variants of the transformation matrix have been used in [17]. The three-phase currents are decomposed into three components, called the balance component ($I_{bn}$), the first unbalance component ($I_{fu}$), and the second unbalanced component ($I_{su}$). The matrix $\mathbf{T}_1 = \mathbf{T}$ is applied to the harmonics with order $h = 3n + 1$ (for an integer number $n \geq 0$). Two other matrices are defined, namely, the matrix $\mathbf{T}_2$ that is applied to the harmonics with order $h = 3n + 2$ and the matrix $\mathbf{T}_0$ that is applied to harmonics with order $h = 3n$ is defined as follows:

$$\mathbf{T}_2 = \frac{1}{3}\begin{vmatrix} 1 & \alpha^2 & \alpha \\ 1 & \alpha & \alpha^2 \\ 1 & 1 & 1 \end{vmatrix},\ \mathbf{T}_0 = \frac{1}{3}\begin{vmatrix} 1 & 1 & 1 \\ 1 & \dfrac{-1-\sqrt{3}}{2} & \dfrac{-1+\sqrt{3}}{2} \\ 1 & \dfrac{-1+\sqrt{3}}{2} & \dfrac{-1-\sqrt{3}}{2} \end{vmatrix}. \tag{11}$$

Considering for each harmonic $h$ the matrix $\mathbf{T}_i$, with $i = \{1,2,0\}$, the transformed currents are [17] as follows:

$$\begin{vmatrix} \bar{I}_{bn}^{(h)} & \bar{I}_{fu}^{(h)} & \bar{I}_{su}^{(h)} \end{vmatrix}^{\mathrm{T}} = \mathbf{T}_i \cdot \begin{vmatrix} \bar{I}_a^{(h)} & \bar{I}_b^{(h)} & \bar{I}_c^{(h)} \end{vmatrix}^{\mathrm{T}}. \tag{12}$$

These transformed components are used to determine the equivalent RMS value of the three-phase current $I_e$

$$I_e^2 = I_{bn1}^2 + I_{u1}^2 + I_{bh}^2 + I_{uh}^2 \tag{13}$$

where the following terms have been defined:

1) current-unbalanced component (first harmonic)

$$I_{u1}^2 = \left(I_{fu}^{(1)}\right)^2 + \left(I_{su}^{(1)}\right)^2 \tag{14}$$

2) current-balanced harmonic component, which is associated with the system balance

$$I_{bh}^2 = \sum_{\substack{h=0 \\ h\neq 1}}^{\infty} \left(I_{bn}^{(h)}\right)^2 \tag{15}$$

3) current unbalanced harmonic component, which is associated with the system unbalance

$$I_{uh}^2 = \sum_{\substack{h=0 \\ h\neq 1}}^{\infty} \left[\left(I_{fu}^{(h)}\right)^2 + \left(I_{su}^{(h)}\right)^2\right]. \tag{16}$$

The equivalent current at the first harmonic [18] is

$$I_{e1} = \sqrt{\left(I_{T1}^{(1)}\right)^2 + \left(I_{T2}^{(1)}\right)^2 + \left(I_{T3}^{(1)}\right)^2}. \tag{17}$$

### B. Current Components not Transformed Into Symmetrical Components

Starting from the RMS three-phase currents defined as

$$I_i = \sqrt{\sum_{h=0}^{\infty} \left(I_i^{(h)}\right)^2} \tag{18}$$

for $i = \{a, b, c, n\}$ representing the phase and neutral conductors, the basic notions are as follows:

1) average absolute current

$$I_{\mathrm{av}} = (I_a + I_b + I_c)/3 \tag{19}$$

2) minimum and maximum currents

$$I_{\min} = \min\{I_a, I_b, I_c\} \tag{20}$$

$$I_{\max} = \max\{I_a, I_b, I_c\} \tag{21}$$

3) equivalent three-phase current [19]

$$I_{\mathrm{eq}} = \sqrt{(I_a^2 + I_b^2 + I_c^2 + I_n^2)/3} \tag{22}$$

4) current deviations [20]

$$d_{I_i} = \frac{1}{I_{\mathrm{eq}}}\sqrt{\left|I_i^2 - I_{\mathrm{eq}}^2\right|}. \tag{23}$$

which measure, for each phase, the difference between the actual waveform and a reference sinusoid whose RMS value is the equivalent three-phase current (22).

### C. Definitions of the Unbalance Indicators

On the basis of the notation that has been introduced previously, the unbalance indicators can be formulated as follows (a synthesis of the information is shown in Table I):

*1) Indicators Defined From Currents Transformed Into Symmetrical Components:* The most popular unbalance indicator is the ratio of negative to positive sequence components, which is determined using the RMS values at the first harmonic, and is known as current unbalance factor (*CUF*) [7]

$$CUF = I_{T2}^{(1)} \Big/ I_{T1}^{(1)}. \tag{24}$$

A further version of the *CUF* can be defined by considering the negative and the positive sequence phasors at the first harmonic, obtaining a complex number called complex current unbalance factor (*CCUF*) [21]

$$\overline{CCUF} = \bar{I}_{T2}^{(1)} \Big/ \bar{I}_{T1}^{(1)}. \tag{25}$$

The previous indicators use only the components at the first harmonic. Some extensions characterize the phase current unbalance for distorted waveforms. The current unbalance indicator (*CUNB*) has been introduced in [18]

$$CUNB = \frac{1}{I_{\mathrm{eq}}}\sqrt{I_{\mathrm{eq}}^2 - \left(I_{T1}^{(1)}\right)^2}. \tag{26}$$

TABLE I
SUMMARY OF THE UNBALANCE INDICATORS

| *acronym* | *name* | *meaning* |
|---|---|---|
| *CCUF* | Complex Current Unbalance Factor | negative sequence to positive sequence ratio (complex values) |
| *CUF* | Current Unbalance Factor | negative sequence to positive sequence ratio (RMS values) |
| *CUI* | Current Unbalance Index | Euclidean sum of the square current deviations w.r.t. equivalent current |
| *CUNB* | Current Unbalance Indicator | relative variation of squared positive sequence w.r.t. equivalent current |
| *ITUD* | Total unbalance with distortion | obtained from dedicated components defined after the SC transformation |
| $TPU_I$ | Total Phase Unbalance | total unbalance to total balance phase current component ratio |
| $U_I$ | Unbalance Indicator | maximum deviation of the RMS phase current w.r.t. average RMS phase current |
| $\delta_{I_i}$ | Absolute current deviation | relative variation of the RMS current at phase *i* w.r.t. average RMS phase current |
| $\varphi_{pI}^{(u)}, \varphi_{pI}^{(ud)}$ | Phase current unbalance factors | unbalance components to fundamental frequency RMS current ratio |

In [17], the indicator of the total current unbalance in the presence of harmonic distortion (*ITUD*) is defined as

$$ITUD = \sqrt{\frac{I_{u1}^2 - I_{uh}^2}{\left(I_{bn}^{(1)}\right)^2 + I_{bh}^2}}. \tag{27}$$

The SCB approach, on the other hand, allows the extension of the typical indicators that are used for the analysis of unbalanced and distorted systems, which defines the indicators referring to the balanced phase current component at fundamental frequency (or including the harmonics). In the first group, they are as follows:

1) phase current-balanced distortion factor

$$\varphi_{pI}^{(bd)} = I_p^{(bd)} \Big/ I_p^{(b1)} \tag{28}$$

2) phase current-unbalanced distortion factor

$$\varphi_{pI}^{(ud)} = I_p^{(ud)} \Big/ I_p^{(b1)} \tag{29}$$

3) phase current overall-unbalanced factor [22]

$$\varphi_{pI}^{(u)} = I_p^{(u)} \Big/ I_p^{(b1)} \tag{30}$$

while the total phase unbalance (*TPU*) indicator refers to the total-balanced phase current component

$$TPU_I = I_p^{(u)} \Big/ I_p^{(b)}. \tag{31}$$

With no harmonic distortion, the indicator $\varphi_{pI}^{(u)}$ becomes equal to the *CUF* (a common indicator of system unbalance). Likewise, the $TPU_I$ indicator extends the unbalance indicator in case of distorted currents. In a perfectly balanced system, $\varphi_{pI}^{(bd)}$ becomes the common total harmonic distortion indicator of the current ($THD_I$).

*2) Indicators Formulated From the Currents not Transformed Into Symmetrical Components:* This set of indicators is composed of

1) unbalance indicator ($U_I$) [7]

$$U_I = \max\left\{\left|I_{\rm av} - I_{\rm min}\right|, \left|I_{\rm max} - I_{\rm av}\right|\right\}/I_{\rm av} \tag{32}$$

2) current unbalance index (*CUI*) [20]

$$CUI = \sqrt{\left(d_{I_a}^2 + d_{I_b}^2 + d_{I_c}^2\right)/3} \tag{33}$$

3) absolute current deviation

$$\delta_{I_i} = |I_i - I_{\rm av}|/|I_{\rm av}| \quad \text{for phases } i = a, b, \text{ and } c. \tag{34}$$

The $U_I$ and *CUI* give total indicators for three-phase systems, allowing for a concise description of the unbalance condition starting from values easily obtainable from a PQ commercial analyzer.

## III. REAL PHOTOVOLTAIC SYSTEM AND STANDARD POWER QUALITY INDICATORS

The real PV system considered has an 834.5-kW$_p$ peak power and is installed on the top of an industrial building in the outskirts of Torino (Italy). It is used partly to supply the local load, partly for power injection into the grid.

The whole PV generator is composed of two different subfields of 778.61 kW$_p$ (integrated into the shed roof) and 55.89 kW$_p$ (non-building integrated) with monocrystalline and polycrystalline silicon modules, respectively (see Fig. 1). All the PV arrays are connected on the LV side through eight three-phase inverters with different power ratings: six for the first section and two for the second one. The inverters and the LV/MV transformer are oversized to minimize losses and maximize lifespan. The total rated powers are 873 kVA for the inverters and 1250 kVA for the $\Delta$/Y transformer. The PV arrays have been installed with the aim to maximize the occupation of the roof surface on the commercial building, accepting the occurrence of partial shading during the day on some arrays. The first field is oriented to the southwest; consequently, the exposure to the solar radiation is neither symmetrical nor optimal and is different during the morning and evening. The second field is optimally (south) oriented and not integrated (less thermal losses). Fig. 2 shows the geometrical layout of the PV arrays. Two PV arrays (no. 4 and 5) are subject to systematic partial shading. These arrays have the same peak power (98 kW$_p$), and their inverters have rated powers of 100 kVA each. The shading patterns that are projected by various obstacles, such as the borders of the triangular-shape shed, differ in the two parts of the day. The array no. 5 is subject to partial shading during the morning (see Fig. 3). The same effect appears on the adjacent array no. 4 during the afternoon when the array no. 5 is no longer shaded.

Even if the architectonic obstructions are not negligible in this case study, the majority of the arrays in the PV system are not subject to shading. In fact, the arrays no. 1, 2, 3, 6, 7, and 8, accounting for a total of 638 kW$_p$, are always exposed to the direct beams in spring and summer during the central sunlight hours (as an example, Fig. 4 shows the *I–V* and *P–V* curves that are measured during the operation of the array no. 1,

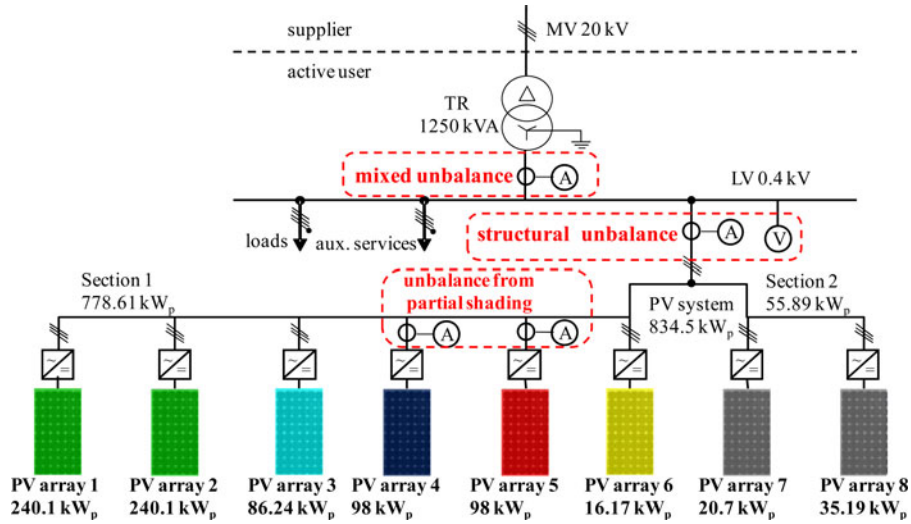


Fig. 1. Electrical scheme of the PV system under study.

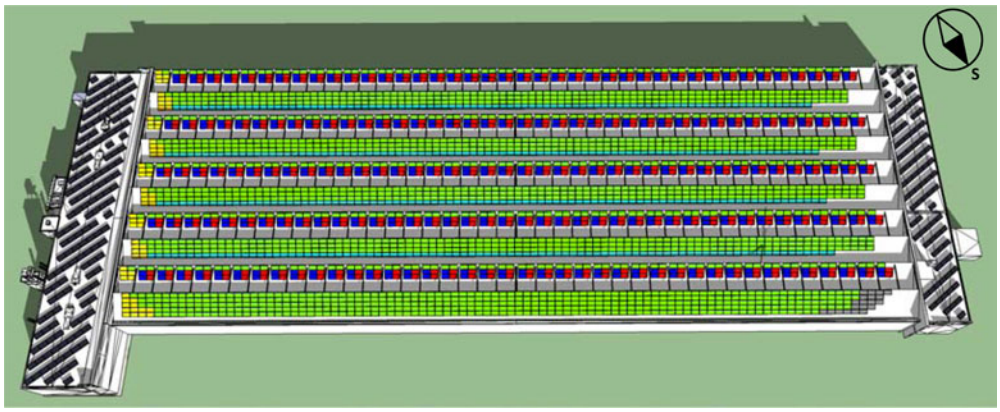


Fig. 2. Geometrical layout of the PV system under study. The colors of the arrays match with the ones indicated in Fig. 1.

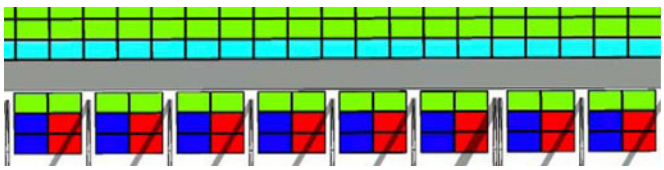

Fig. 3. Particular of the partial shading over the 98 $kW_p$ PV array no. 5 at hour 12:15 A.M. in January.

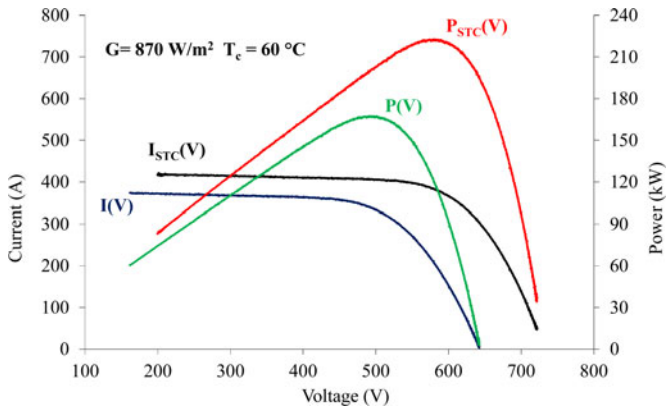


Fig. 4. Experimental results (*I–V* and *P–V* curves) on PV array no. 1 with 240 $kW_p$ on a Spring day. Actual data and values reported to the standard test conditions.

which indicates that no shading occurs). In order to study the PQ impact of this PV plant on the grid, a first experimental campaign has been conducted by means of a standard PQ analyzer [23], during eight consecutive days in July. Figs. 5 and 6 represent the evolution of the current and voltage unbalance (*CUF*, *VUF*[1]) and their *THD* with respect to the output active power of the whole PV system for a day with clear sky.

Around the maximum active power level, the unbalance and the harmonic distortion are below the technical thresholds [24], [25], since $VUF < 0.2\%$, $CUF < 3\%$, $THD_V < 1\%$, and $THD_I < 5\%$. Conversely, at low-power level in the morning and in the evening, the current distortion and unbalance increase, with a slight worsening in the evening compared with the morning. This behavior has been regularly detected in the tests carried out on the system. Focusing our attention on the current unbalance, this can be caused by the different evolutions of the

[1]The voltage unbalance factor (VUF) is defined as the ratio between the negative and the positive sequence components of the voltage [7].

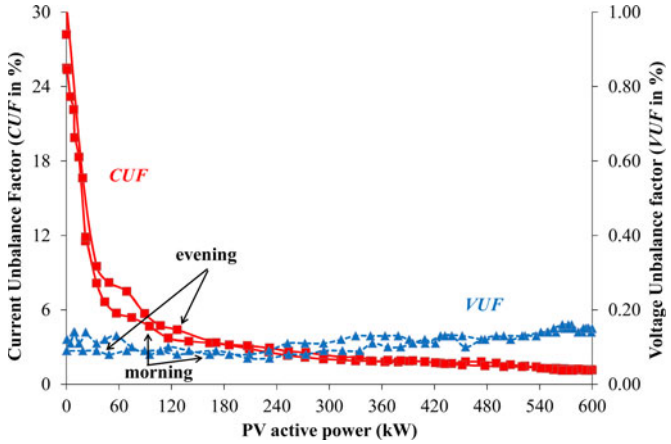


Fig. 5. Evolution of the *CUF* and *VUF*, during a day in July, under clear sky conditions.

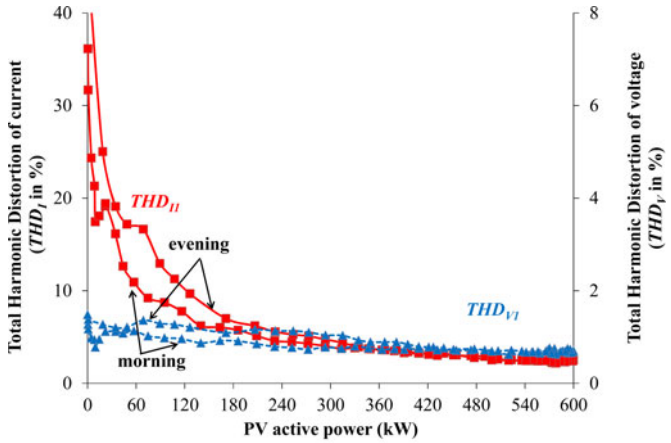


Fig. 6. Evolution of the $THD_I$ and $THD_V$ for the first phase, during the day in July, under clear sky conditions.

shade projected by the shed profile over the PV arrays. The uneven exposure to the solar irradiance among the PV arrays and the partial shading of some of them are sources of unbalance. The harmonic distortion is greater in the evening, which suggests that during the last hours of the day the mismatch in solar irradiance between the exposed and shaded areas is more marked than in the morning.

The standard PQ indices do not quantify how much the harmonic distortion does contribute to unbalance, nor to what extent harmonic distortion is affected by the system unbalance. The unbalance indicators that are described in the previous section are then applied to the output currents of the three-phase inverters of the PV system.

In the following section, the PQ analysis is discussed for the whole PV system in high solar irradiance to verify the reference values of the unbalance indicators due to "structural unbalance." This first analysis does not highlight the partial shading phenomenon, which affects only some of the PV arrays. The roof of the building is the typical triangular-shape shed and presents tie-beams which strengthen the top structure but create a periodic shading over some PV arrays in the early morning and in the afternoon [26]. The shade evolution causes a diagonal partial

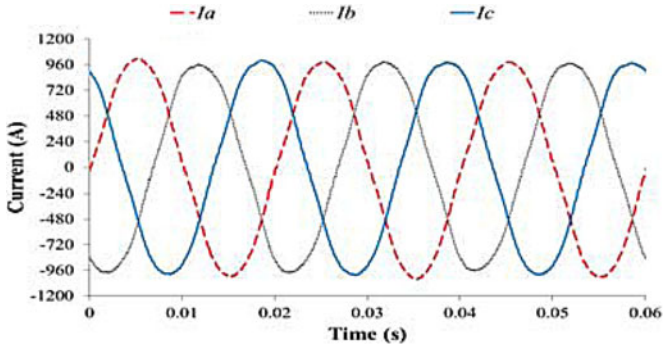


Fig. 7. Three-phase output currents of the PV system with high solar irradiance (at 16:20 in May 2013).

shading over the modules, like a series of moving rod-shaped shades (see Fig. 3). Unbalance is studied for the two arrays that are affected by partial shading.

Thus, the condition of "mixed unbalance" is considered, taking into account the point of common coupling (PCC), where unbalance is also due to different load currents for each phase absorbed by the internal building services. The structure is a clothing wholesale warehouse with nonlinear loads (fluorescent lamps, since the illumination is guaranteed from 8:00 A.M. to 8:00 P.M.; machines for air conditioning; personal computers; and a data processing center).

## IV. Experimental Results

### A. Structural Unbalance

Several sampled ten-cycle waveforms for each line voltage and current of the three-phase output of the whole PV system have been gathered near the transformer. The measurements have been carried out in the afternoon of a day in May, from 4:00 to 4:20 P.M., with high average solar irradiance, which is slightly above 950 W/m$^2$. Fig. 7 shows the currents that are measured in the last acquisition, at around 900 W/m$^2$ of solar irradiance and an active power output almost equal to 60% of the rated power of all inverters and 40% with respect to the transformer rated power. This means that the BIPV system, which is considered nearly at full power, works at less than 60% of its potential, because of its suboptimal exposure, presence of obstacles, and the temperature effects. Moreover, the inverters and the transformer are far away to be fully loaded.

As illustrated in Fig. 8, the total three-phase instantaneous power is not constant due to unbalance among the phases, with power of phase *b* smaller than the others (i.e., 3.5 kW or –2% with respect to the average active power of the single phases). This "structural unbalance" is not remarkable, since all the currents are generated by three-phase inverters in high solar irradiance conditions.

Table II reports the average values of the indicators computed. The SC current components reveal that the unbalance at the fundamental frequency (from the *CUF* value) is around 1%. This is confirmed by the *CUNB*, slightly increasing due to waveform distortion.

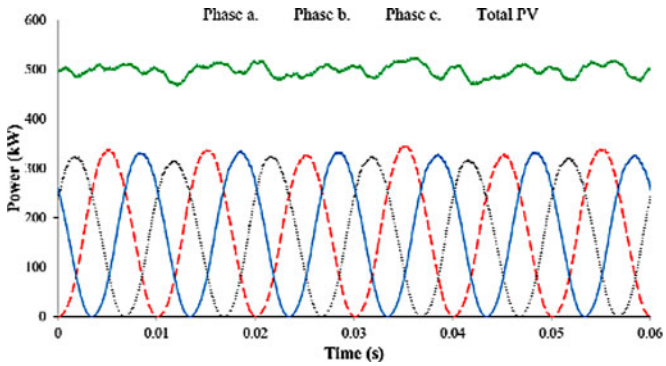


Fig. 8. Output power for the three phases and the total PV system, with high solar irradiance and no shading (at hour 16:20 in May 2013).

TABLE II
CURRENT COMPONENTS AND UNBALANCE INDICATORS IN THE CASE OF STRUCTURAL UNBALANCE

| Indicators from SC values | | | |
|---|---|---|---|
| Current Component | | Unbalance Indicator | |
| $I_p^{(b)}$ [A] | 745.69 | *CUF* [p.u.] | 0.012 |
| $I_p^{(b1)}$ [A] | 745.43 | ∠*CCUF* [rad] | -0.760 |
| $I_p^{(bd)}$ [A] | 19.28 | *CUNB* [p.u.] | 0.013 |
| $I_p^{(u)}$ [A] | 10.01 | $\varphi_{pI}^{(u)}$ | 0.016 |
| $I_p^{(u1)}$ [A] | 8.27 | $\varphi_{pI}^{(ud)}$ | 0.009 |
| $I_p^{(ud)}$ [A] | 6.52 | $TPU_I$ [p.u.] | 0.016 |
| $I_p^{(d)}$ [A] | 20.36 | *ITUD* [p.u.] | 0.016 |
| **Indicators from non-SC values** | | | |
| Current Component | | Unbalance Indicator | |
| $I_{eq}$ [A] | 746.40 | $U_I$ [p.u.] | 0.02 |
| $d_{Ia}$ [p.u.] | 0.14 | *CUI* [p.u.] | 0.14 |
| $d_{Ib}$ [p.u.] | 0.18 | $\delta_{Ia}$ [p.u.] | 0.01 |
| $d_{Ic}$ [p.u.] | 0.11 | $\delta_{Ib}$ [p.u.] | 0.02 |
| $I_a$ [A] | 753.27 | $\delta_{Ic}$ [p.u.] | 0.01 |
| $I_b$ [A] | 734.39 | | |
| $I_c$ [A] | 751.10 | | |
| $I_{av}$ [A] | 746.25 | | |

The relatively low weight of the harmonic distortion on the unbalance is confirmed by comparing the values of $\varphi_{pI}^{(u)}$ and $\varphi_{pI}^{(ud)}$, which are 1.6% for the overall factor and only 0.9% if the fundamental frequency is excluded by the evaluation of the unbalance component of the phase current. Moreover, $\varphi_{pI}^{(u)}$ is equal to $TPU_I$, at least at the third decimal digit, since $I_p^{(b1)}$ is close to $I_p^{(b)}$, just because the harmonic distortion is small. The $THD_I$ values of the phases are estimated with an average of 2.62%, 2.81%, and 2.76%, while the value of $\varphi_{pI}^{(bd)}$, which is not shown in Table II, is close (2.6%), meaning that the small unbalance has slight influence on the harmonic distortion.

The alternative current decomposition method shows that the unbalance indicator $U_I$ confirms a value around 2%, as well as the absolute current deviations state a disagreement of the RMS values of the phase currents from the value $I_{\rm av}$ of around 1–2%. The *CUI* is 14%, which reveals that this indicator gives

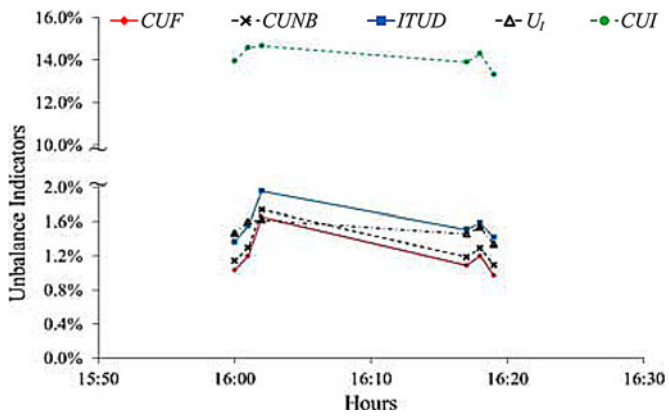


Fig. 9. Unbalance indicators versus time in case of structural unbalance. The *ITUD* and $TPU_I$ values are equal.

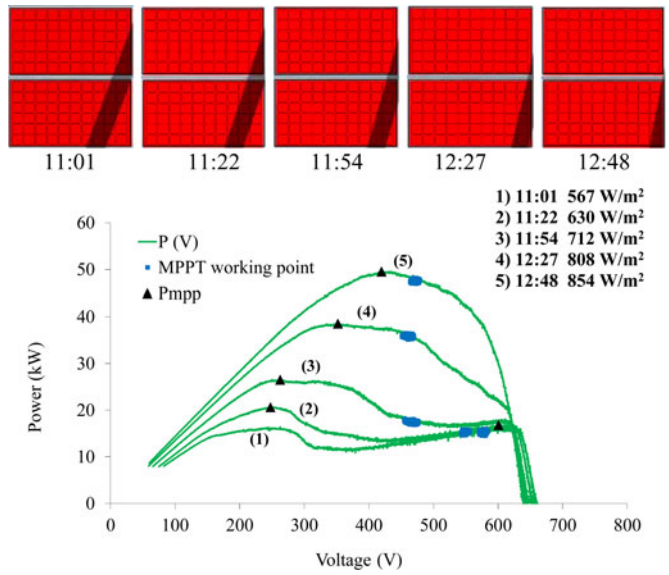


Fig. 10. Time evolution of the *P–V* curves and of the shading over the array no. 5 in the late morning of a day in July 2012 (the hours are indicated under the corresponding pair of PV modules).

the highest values. The absolute current deviations allow the identification of the phase that contributes the most to unbalance. The time evolution of the unbalance indicators is almost constant, since the solar irradiance and the shading do not vary very much during the measurements (see Fig. 9).

### B. Unbalance From Partial Shading

Two PV arrays subject to the described partial shading and their three-phase 100-kVA inverters are considered. The first one (array no. 5), with a 98-kW$_p$ peak power, is shaded in the morning and, when the measurements were performed in January, the partial shading lasted until the early hours of the afternoon. The partial shading generates a significant distortion in the shape of the *I–V* curve and makes the maximum power point (MPP) tracker fail, giving variable instantaneous power in the *P–V* curve (see Fig. 10) and unbalance in the three-phase current waveforms. Here, the MPP tracker (MPPT) is not able to extend the search of the MPP down to the voltage of the

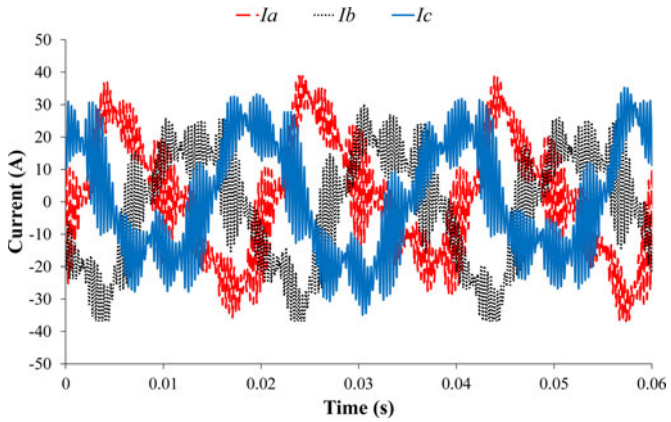


Fig. 11. Three-phase output currents of the array-5 inverter with partial shading (at 2 P.M. in January 2012).

TABLE III
CURRENT COMPONENTS AND UNBALANCE INDICATORS IN THE CASE OF PARTIAL SHADING OF PV ARRAY NO. 4

| Indicators from SC values | | | | |
|---|---|---|---|---|
| Current Component | | | Unbalance Indicator | |
| $I_p^{(b)}$ [A] | 18.82 | | $CUF$ [p.u.] | 0.107 |
| $I_p^{(b1)}$ [A] | 18.68 | | $\angle CCUF$ [rad] | 0.980 |
| $I_p^{(bd)}$ [A] | 2.34 | | $CUNB$ [p.u.] | 0.106 |
| $I_p^{(u)}$ [A] | 2.84 | | $\varphi_{pI}^{(u)}$ | 0.153 |
| $I_p^{(u1)}$ [A] | 1.97 | | $\varphi_{pI}^{(ud)}$ | 0.109 |
| $I_p^{(ud)}$ [A] | 2.02 | | $TPU_I$ [p.u.] | 0.152 |
| $I_p^{(d)}$ [A] | 3.10 | | $ITUD$ [p.u.] | 0.152 |
| Indicators from non-SC values | | | | |
| Current Component | | | Unbalance Indicator | |
| $I_{eq}$ [A] | 19.91 | | $U_I$ [p.u.] | 0.09 |
| $d_{Ia}$ [p.u.] | 0.29 | | $CUI$ [p.u.] | 0.35 |
| $d_{Ib}$ [p.u.] | 0.30 | | $\delta_{Ia}$ [p.u.] | 0.05 |
| $d_{Ic}$ [p.u.] | 0.42 | | $\delta_{Ib}$ [p.u.] | 0.05 |
| $I_a$ [A] | 20.78 | | $\delta_{Ic}$ [p.u.] | 0.09 |
| $I_b$ [A] | 20.80 | | | |
| $I_c$ [A] | 18.03 | | | |
| $I_{av}$ [A] | 19.87 | | | |

global MPP, even if the distances between the global MPP and the operating points of the MPPT are progressively decreasing with the reduction of the shading. The shading pattern involves a few cells in the modules and the bypass diodes, exhibiting the typical changes of slope in *P–V* curves, work to limit the power losses.

Many ten-cycle waveforms have been sampled for each line voltage and current from 12:15 A.M. to 2 P.M. Fig. 11 reports the currents gathered in the last measurement, with an average solar irradiance of 354 W/m$^2$. The output active power is 10% of the inverter's rated power. The second array (no. 4), with peak power 98 kW$_p$, is affected by partial shading in the afternoon. The signal acquisition took place on an April day from 5 to 6 P.M., with an average solar irradiance of 560 W/m$^2$. Again, the output active power is 10% of the inverter's rated power. Tables III and

TABLE IV
CURRENT COMPONENTS AND UNBALANCE INDICATORS IN THE CASE OF PARTIAL SHADING OF PV ARRAY NO. 5

| Indicators from SC values | | | | |
|---|---|---|---|---|
| Current Component | | | Unbalance Indicator | |
| $I_p^{(b)}$ [A] | 12.08 | | $CUF$ [p.u.] | 0.113 |
| $I_p^{(b1)}$ [A] | 11.92 | | $\angle CCUF$ [rad] | 3.368 |
| $I_p^{(bd)}$ [A] | 1.90 | | $CUNB$ [p.u.] | 0.113 |
| $I_p^{(u)}$ [A] | 1.98 | | $\varphi_{pI}^{(u)}$ | 0.168 |
| $I_p^{(u1)}$ [A] | 1.33 | | $\varphi_{pI}^{(ud)}$ | 0.122 |
| $I_p^{(ud)}$ [A] | 1.45 | | $TPU_I$ [p.u.] | 0.166 |
| $I_p^{(d)}$ [A] | 2.39 | | $ITUD$ [p.u.] | 0.166 |
| Indicators from non-SC values | | | | |
| Current Component | | | Unbalance Indicator | |
| $I_{eq}$ [A] | 14.61 | | $U_I$ [p.u.] | 0.10 |
| $d_{Ia}$ [p.u.] | 0.48 | | $CUI$ [p.u.] | 0.34 |
| $d_{Ib}$ [p.u.] | 0.21 | | $\delta_{Ia}$ [p.u.] | 0.10 |
| $d_{Ic}$ [p.u.] | 0.21 | | $\delta_{Ib}$ [p.u.] | 0.04 |
| $I_a$ [A] | 12.73 | | $\delta_{Ic}$ [p.u.] | 0.06 |
| $I_b$ [A] | 14.67 | | | |
| $I_c$ [A] | 14.98 | | | |
| $I_{av}$ [A] | 14.13 | | | |

IV report the average values of the current components and unbalance indicators for the output currents of both selected inverters, which are calculated with the two methods of current decomposition for each measure.

The indicators that are calculated from SC values reveal that the unbalance at the fundamental frequency is around 11% (CUF). This is confirmed by the *CUNB*, which should take into account the waveform distortion. The harmonic content of the currents is not negligible, as it can be verified by the distortion components $I_p^{(bd)}$ and $I_p^{(ud)}$, whose ratios to $I_p^{(b1)}$, i.e., $\varphi_{pI}^{(bd)}$ and $\varphi_{pI}^{(ud)}$, are around 16% and 12%, respectively, for the inverter of the array no. 5, and 13% and 11% for the inverter of the array no. 4. Therefore, a better evaluation of the impact of the harmonic distortion over the currents' unbalance is given by the $TPU_I$, around 17% for the inverter of the array no. 5 and 15% for the inverter of the array no. 4 (the same values are obtained for the indicator *ITUD*). The overall unbalance $\varphi_{pI}^{(u)}$ is very close to the $TPU_I$, but it is slightly greater because $I_p^{(b1)}$ is smaller than $I_p^{(b)}$ due to distortion.

From the other set of indicators, the unbalance indicator $(U_I)$ confirms a value around 10% for the inverter of the array no. 5 and 9% for the inverter of the array no. 4. The current deviations for the array no. 5 reveal a disagreement of the RMS values of the phase currents from the equivalent value $I_{\rm eq}$, which is larger for phase $a$ with respect to the other phases. This situation is confirmed also by the absolute current deviations, which considers the average value instead of $I_{\rm eq}$ and gives a value of *CUI* equal to 34%. For the inverter of the array no. 4, the phases $a$ and $b$ are more aligned, while phase $c$ deviates more from the $I_{\rm eq}$ and $I_{\rm av}$ values. The *CUI* is very similar as for the inverter of the array no. 5 (35%).

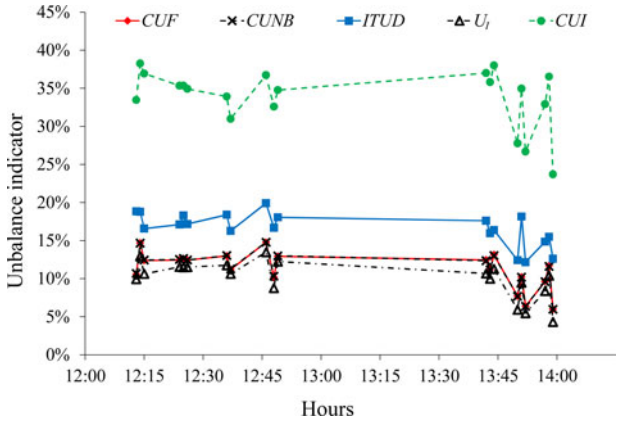


Fig. 12. Unbalance indicators versus time with partial shading in the early afternoon (array no. 5). The *ITUD* and $TPU_I$ values are equal.

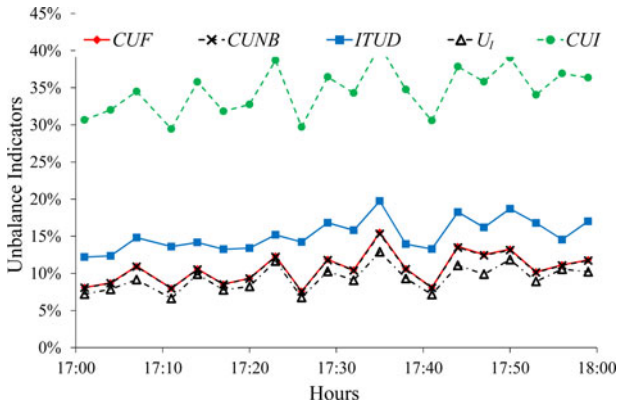


Fig. 13. Unbalance indicators versus time with partial shading in the afternoon (array no. 4). The *ITUD* and $TPU_I$ values are equal.

In Fig. 12, the time evolution of the unbalance indicators for PV array no. 5 is illustrated as the partial shading decreases. Conversely, the increase of the shading over the PV array no. 4 is reflected on the slight rise of the unbalance indicators versus time, as shown in Fig. 13.

### C. Mixed Unbalance

When the total three-phase currents that are exchanged with the grid (seen from the distribution transformer) are studied, the situation changes drastically. The signals are gathered from the data acquisition system located just before the transformer around 1:00 P.M. in June (see Fig. 14). During each measurement, the general circuit breaker of the PV plant has been opened. Sampling ten cycles of the waveforms before and after the breaker opening, the total three phase currents that are exchanged with the grid have been obtained with the PV system connected (see Fig. 15) and without it (see Fig. 16). When the circuit breaker is closed, the power that is injected into the grid is 18% of the inverters' rated power and 13% of the transformer rated power. The PV generator currents are reconstructed applying the Kirchhoff's law at the current node, making the approximation that the load currents do not change before and after the opening. The overall active power at PV output results around 26% of the inverters' rated power and 18% of the transformer

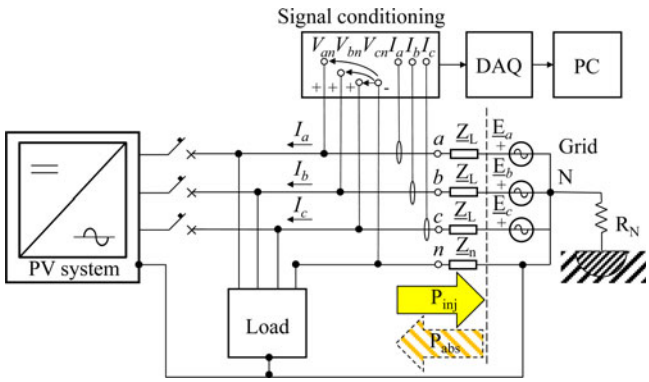


Fig. 14. Scheme of the three-phase system for signals acquisition.

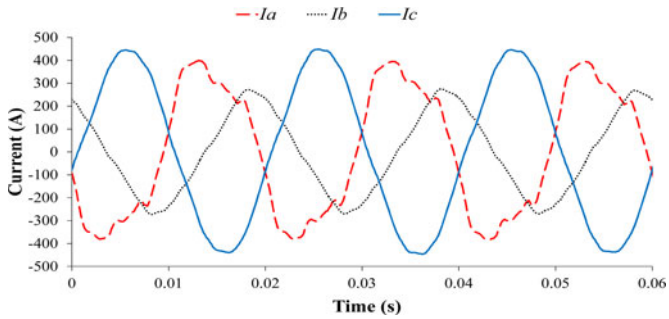


Fig. 15. Three-phase currents at the PCC with the PV system connected (hour 14:05 in June).

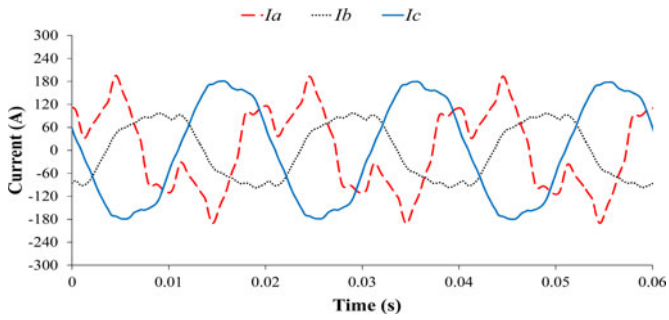


Fig. 16. Three-phase currents absorbed at the PCC, without PV system (hour 14:05 in June).

rated power. This can be considered to be an average operating condition of the PV system, i.e., the PV output power is nearly 40% of that with high irradiance. Moreover, this allows us to appreciate the influence of the load currents. When the circuit breaker is open, the loads are absorbing around 8% of the inverter's rated power and 5% of the transformer rated power. The PQ analysis is performed for the total currents exchanged when the breaker is closed.

The unbalance indicators (see Table V) are very high. The *CUF* is around 0.36, while $TPU_I$ and *ITUD* are around 0.38, as for the overall unbalance factor $\varphi_{pI}^{(u)}$. This means that the harmonic distortion has its influence on unbalance. However, this influence is very low compared with the one occurring in case of partial shading. Furthermore, the values of $\varphi_{pI}^{(bd)}$ and $\varphi_{pI}^{(ud)}$ are nearly 0.1, which are remarkably lower than $\varphi_{pI}^{(u)}$,

TABLE V
CURRENT COMPONENTS AND UNBALANCE INDICATORS IN THE CASE OF MIXED UNBALANCE

| Indicators from SC values | | | |
|---|---|---|---|
| Current Component | | Unbalance Indicator | |
| $I_p^{(b)}$ [A] | 230.92 | *CUF* [p.u.] | 0.363 |
| $I_p^{(b1)}$ [A] | 229.78 | $\angle CCUF$ [rad] | -1.518 |
| $I_p^{(bd)}$ [A] | 22.86 | *CUNB* [p.u.] | 0.344 |
| $I_p^{(u)}$ [A] | 86.80 | $\varphi_{pI}^{(u)}$ | 0.378 |
| $I_p^{(u1)}$ [A] | 84.04 | $\varphi_{pI}^{(ud)}$ | 0.095 |
| $I_p^{(ud)}$ [A] | 21.70 | $TPU_I$ [p.u.] | 0.376 |
| $I_p^{(d)}$ [A] | 31.52 | *ITUD* [p.u.] | 0.376 |
| **Indicators from non-SC values** | | | |
| Current Component | | Unbalance Indicator | |
| $I_{eq}$ [A] | 250.49 | $U_I$ [p.u.] | 0.30 |
| $d_{Ia}$ [p.u.] | 0.30 | *CUI* [p.u.] | 0.58 |
| $d_{Ib}$ [p.u.] | 0.74 | $\delta_{Ia}$ [p.u.] | 0.09 |
| $d_{Ic}$ [p.u.] | 0.60 | $\delta_{Ib}$ [p.u.] | 0.30 |
| $I_a$ [A] | 262.00 | $\delta_{Ic}$ [p.u.] | 0.21 |
| $I_b$ [A] | 167.90 | | |
| $I_c$ [A] | 292.91 | | |
| $I_{av}$ [A] | 240.93 | | |

and $I_p^{(u1)}$ is much greater than $I_p^{(ud)}$; all of this indicates that the unbalance is mainly due to the component at fundamental frequency. The other decomposition method gives an unbalance indicator of 30% and a *CUI* of 58%. The current and absolute deviations report that the phase $b$ deviates more than the other two phases from the equivalent and average value.

## V. SUGGESTIONS FOR EXTENDING THE UNBALANCE INDICATORS IN POWER QUALITY STANDARDS

The results that are obtained can be useful to promote changes in the current standards in order to account for the dependence of the unbalance components on harmonic distortion in the formulation of the unbalance indicators. On these bases, the values that are obtained in the application studied can provide some hints.

The effectiveness of introducing a new indicator in the standards can be discussed by considering the *CUF* as the traditional reference. The unbalance indicators $TPU_I$ and *ITUD* are the most suitable ones, as they can take into proper account the presence of distortion together with unbalance, providing values realistically higher than the *CUF* in a way depending on harmonic distortion, and becoming equal to the *CUF* when harmonic distortion is absent.

The other indicators may be considered to be less effective. In fact, the values of the *CUNB* indicator are relatively similar to those of the *CUF* and, as such, could not highlight the effect of harmonic distortion in a sufficient way. Moreover, the *CUI* and $U_I$ indicators have the potential advantage of being easy to be calculated from the RMS values of the phase and neutral currents, without requiring the SC transformation. However, in the presence of harmonic distortion, the $U_I$ values could become lower than the traditional *CUF* values (making the $U_I$ less appropriate), while the *CUI* values may be significantly higher than the *CUF* (even of one order of magnitude, as in Table II) which are also in the presence of relatively small unbalance, and are numerically too large with respect to the values traditionally handled by the operators.

From the results that are obtained, a possible limit on $TPU_I$ or *ITUD* for the whole PV system could be indicatively set up to a value in the range 0.1–0.2. The values of the limit can be further detailed taking into account the ratio of the peak power of the PV system to the size of the distribution transformer, with lower $TPU_I$ or *ITUD* limit for higher values of that ratio. This way, it is expected that a PV system with moderate structural unbalance does not exceed the limit, while a PV system subject to consistent partial shading would need some modifications in the placement of the arrays (e.g., reducing the surface covered by the PV modules) to avoid negative effects on harmonic distortion and unbalance.

## VI. CONCLUSIONS

The operating conditions of PV systems may lead to the occurrence of different types of unbalance of the currents in the three-phase system. This paper has proposed a categorization of unbalance into three basic types: structural unbalance, unbalance from partial shading, and mixed unbalance. For each type of unbalance, results from experimental analyses have highlighted that the unbalance in a PV system cannot be considered negligible in the presence of structural issues and can become more relevant with partial shading and unbalanced distorted loads. This aspect is important to design a PV system and its grid connection, oversizing the distribution transformer if needed.

A number of indicators taken from the reviewed literature have been calculated. Some indicators are computed to allow the direct use of the parameters that are provided by commercial PQ analyzer. The SCB method leads to concise three-phase indicators, making it possible to identify various unbalance components also in the presence of harmonic distortion of the current waveforms.

Two unbalance indicators ($TPU_I$ and *ITUD*) have been found to be particularly appropriate to represent the phase current unbalance in the presence of distorted waveforms, extending the indicators included in the present standards.

Setting up the limits in the standards is a matter of discussion inside the standardization bodies. According to the present trend of formulation of the standards, the PQ indicators are not assessed individually, but they consider the values of the indicator that are obtained from a number of successive measurements during a predefined time period and take, for example, the 95th percentile (i.e., the 95% nonexceeding probability) from the cumulative distribution of the values of the indicator as the number characterizing the system under test. The acceptability limit is then defined on the 95th percentile. This assessment is directly applicable to the $TPU_I$ and *ITUD* values as well.

## ACKNOWLEDGMENT

The authors would like to thank Prof. Petru Postolache and Prof. Cornel Toader of the Universitatea Politehnica din Bucureşti, Bucharest, Romania, as well as Mr. Guido Guerra,

Omnianet s.r.l. (designer and installer of the studied PV system), for their insightful discussions.

## REFERENCES


[1] IEA PVPS Task 1, "Trends in photovoltaic applications survey report of selected IEA countries between 1992 and 2012," pp. 1–46, 2013.

[2] G. Chicco, J. Schlabbach, and F. Spertino, "Experimental assessment of the waveform distortion in grid-connected photovoltaic installations," *Sol. Energy*, vol. 83, no. 7, pp. 1026–1039, Jul. 2009.

[3] C. L. Fortescue, "Method of symmetrical coordinates applied to the solution of polyphase networks," *Trans. AIEE*, vol. 37, pp. 1027–1140, 1918.

[4] NEMA—MG1-Section II—Performance Standards Applying to All Machines. Part 14, NEMA Std. Pub. MG1-1993, 1993.

[5] T. Kerekes, R. Teodorescu, M. Liserre, C. Klumpner, and M. Sumner, "Evaluation of three-phase transformerless photovoltaic inverter topologies," *IEEE Trans. Power Electron.*, vol. 24, no. 9, pp. 2202–2211, Sep. 2009.

[6] K. Lee, T. M. Jahns, T. A. Lipo, V. Blasko, and R. D. Lorenz, "Observer-Based control methods for combined source-voltage harmonics and unbalance disturbances in PWM voltage-source converters," *IEEE Trans. Ind. Appl.*, vol. 45, no. 6, pp. 2010–2021, Nov./Dec. 2009.

[7] *IEEE Recommended Practice for Electric Power Distribution for Industrial Plants*, IEEE Std. 141-1993, Apr. 29, 1994.

[8] R. Yan and T. K. Saha, "Voltage variation sensitivity analysis for unbalanced distribution networks due to photovoltaic power fluctuations," *IEEE Trans. Power Syst.*, vol. 27, no. 2, pp. 1078–1089, May 2012.

[9] S. X. Duarte and N. Kagan, "A power-quality index to assess the impact of voltage harmonic distortions and unbalance to three-phase induction motors," *IEEE Trans. Power Del.*, vol. 25, no. 3, pp. 1846–1854, Jul. 2010.

[10] A. E. Emanuel, "On the definition of power factor and apparent power in unbalanced polyphase circuits with sinusoidal voltage and currents," *IEEE Trans. Power Del.*, vol. 8, no. 3, pp. 841–847, Jul. 1993.

[11] B. Mahdad, K. Srairi, and T. Bouktir, "Optimal power flow for large-scale power system with shunt facts using efficient parallel Ga," *Electr. Power Energy Syst.*, vol. 32, no. 5, pp. 507–517, 2010.

[12] S. Segui-Chilet, F. J. Gimeno-Sales, S. Orts, G. Garcera, E. Figueres, M. Alcaniz, and R. Masot, "Approach to unbalance power active compensation under linear load unbalances and fundamental voltage asymmetries," *Electr. Power Energy Syst.*, vol. 29, no. 7, pp. 526–39, 2007.

[13] N. Femia, G. Petrone, G. Spagnuolo, and M. Vitelli, *Power Electronics and Control Techniques for Maximum Energy Harvesting in Photovoltaic Systems*. Boca Raton, FL, USA: CRC, 2013.

[14] F. Spertino, J. Sumaili, H. Andrei, and G. Chicco, "PV module parameter characterization from the transient charge of an external capacitor," *IEEE J. Photovoltaics*, vol. 3, no. 4, pp. 1325–1333, Oct. 2013.

[15] G. Chicco, P. Postolache, and C. Toader, "Analysis of three-phase systems with neutral under distorted and unbalanced conditions in the symmetrical component-based framework," *IEEE Trans. Power Del.*, vol. 22, no. 1, pp. 674–683, Jan. 2007.

[16] G. Chicco, P. Postolache, and C. Toader, "Triplen harmonics: Myths and reality," *Elect. Power Syst. Res.*, vol. 81, no. 7, pp. 1541–1549, Jul. 2011.

[17] T. Zheng, E. B. Makram, and A. A. Girgis, "Evaluating power system unbalance in the presence of harmonic distortion," *IEEE Trans. Power Del.*, vol. 18, no. 2, pp. 393–397, Apr. 2003.

[18] D. Sharon, J. C. Montaño, A. Lopez, M. Castilla, D. Borras, and J. Gutierrez, "Power quality factor for networks supplying unbalanced nonlinear loads," *IEEE Trans. Instrum. Meas.*, vol. 57, no. 6, pp. 1268–1274, Jun. 2008.

[19] R. Arsenau, Y. Baghzouz, J. Belanger, K. Bowes, A. Braun, A. Chiaravallo, M. Cox, S. Crampton, A. Emanuel, P. Filipski, E. Gunther, A. Girgis, D. Hartmann, S.-D. He, G. Hensley, D. Iwanusiw, W. Kortebein, T. McComb, A. McEachern, T. Nelson, N. Oldham, D. Piehl, K. Srinivasan, R. Stevens, T. Unruh, and D. Williams, "Practical definitions for powers in systems with nonsinusoidal waveforms and unbalanced loads: A discussion," *IEEE Trans. Power Del.*, vol. 11, no. 1, pp. 79–101, Jan. 1996.

[20] P. Salmerón, R. S. Herrera, A. Pérez Vallés, and J. Prieto, "New distortion and unbalance indices based on power quality analyzer measurements," *IEEE Trans. Power Del.*, vol. 24, no. 2, pp. 501–507, Apr. 2009.

[21] Y. Wang, "Analysis of effects of three-phase voltage unbalance on induction motors with emphasis on the angle of the complex voltage unbalance factor," *IEEE Trans. Energy Convers.*, vol. 16, no. 3, pp. 270–275, Sep. 2001.

[22] A. Dell'Aquila, M. Marinelli, V. G. Monopoli, and P. Zanchetta, "New power-quality assessment criteria for supply systems under unbalanced and nonsinusoidal conditions," *IEEE Trans. Power Del.*, vol. 19, no. 3, pp. 1284–1290, Jul. 2004.

[23] *Int. Electrotech. Comm., Electromagnetic compatibility (EMC) – Part 4-30: Testing and measurement techniques—Power quality measurement methods*, IEC Std. 61000-4-30 Ed.2, 2007.

[24] *Eur. Std., Voltage Characteristics of Electricity Supplied by Public Distribution Networks*, EN 50160:2010-12, 2010.

[25] *Int. Electrotech. Comm., Photovoltaic systems: characteristics of the utility interface*, IEC Std. 1727, 1995.

[26] F. Spertino, P. Di Leo, and F. Corona, "Inverters for grid connection of photovoltaic systems and power quality: case studies," in *Proc. IEEE 3rd Int. Symp. Power Electron. Distrib. Generation Syst.*, Aalborg, Denmark, Jun. 25–28, 2012, pp. 564–569.


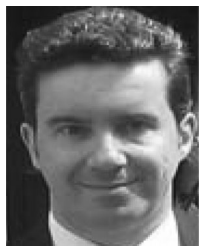

**Gianfranco Chicco** (M'98–SM'08) received the Ph.D. degree in electrotechnics engineering from Politecnico di Torino (PdT), Torino, Italy, in 1992.

He is currently a Professor of electrical energy systems with the Energy Department, PdT. His research interests include power system and distribution system analysis, energy efficiency, multigeneration, load management, artificial intelligence applications, and power quality.

Dr. Chicco is a Member of the Italian Association of Electrical, Electronic, and Telecommunications Engineers.

**Fabio Corona** received the M.Sc. degree in electronics engineering from Università degli Studi "Roma Tre," Roma, Italy, in 2001. He is currently working toward the Ph.D. degree in electrical engineering with the Energy Department, Politecnico di Torino, Torino, Italy.

His work expertise, as an Italian Army officer, involves military-equipment procurement and maintenance. His area of interest includes simulation and experimental testing on grid-connected photovoltaic systems, distributed generation, and related power quality issues.

**Radu Porumb** (M'10) received the Ph.D. degree in electrical engineering from Politecnico di Torino, Torino, Italy, in 2005.

He is currently a Lecturer of electrical energy systems with the Universitatea Politehnica din Bucureşti, Bucharest, Romania. His research interests include distribution system analysis, load management, energy efficiency, and power quality.

**Filippo Spertino** (M'07) received the Ph.D. degree in electrical engineering from Politecnico di Torino (PdT), Torino, Italy, in 2000.

He is currently an Assistant Professor of electric power systems and renewable energy systems with the Energy Department, PdT. His research interests include the design, simulation, and experimental testing on photovoltaic and wind energy systems, as well as instrument calibration.

Dr. Spertino is a Member of the Italian Association of Electrical, Electronic, and Telecommunications Engineers and the Italian Electrotechnical Committee.